Instabilities of coupled density fronts and their nonlinear evolution in the two-layer rotating shallow water model. Influence of the lower layer and of the topography.

B. Ribstein and V. Zeitlin

Laboratory of Dynamical Meteorology, Univ. P.et M. Curie, Paris, France

Sub-mesoscale Ocean Processes, Toronto 2013

Plan

Density fronts reminder

Density fronts:

- ubiquitous in nature and easy to reproduce in the lab
- characteristically unstable
- following classics (Griffiths, Killworth & Stern, 1982), the instabilities of DF are traditionnally studied in the framework of 1- or 2-layer rotating shallow water (RSW) models ; result from phase-locking and resonance of characteristic frontal waves
- recent progress: detailed numerical linear stability analysis and high-resolution DNS of nonlinear saturation (Gula, Zeitlin & Bouchut, 2010).

Motivation

Not well- understood:

- the role of the bottom layer
- the role of topography
- details nonlinear saturation

Main motivation:

To investigate how the classical instability of the double density fronts, resulting from a resonance between two frontal waves propagating along the respective fronts, interacts with other long-wave instabilities appearing due to the active lower layer and topography and, respectively, Rossby and topographic waves which are activated in the system.

Goals

We want:

- to give a complete classification of the instabilities of double density fronts in the presence of an active lower layer and shelf-like topography
- to intercompare them and to identify the dominant one and possible instability swaps in the parameter space
- to identify and intercompare different saturation patterns

Program realized in:

Ribstein & Zeitlin, 2013, J. Fluid Mech., **716**, 528 - 565.

Methodology and tools

We follow previous work (Scherer & Zeitlin 2008; Gula & Zeitlin 2010; Gula, Zeitlin & Bouchut 2010) and add combined effects of baroclinicity and bottom topography:

- Density fronts: 2-layer RSW with outcropping interface.
- Topography: escarpment beneath the upper-layer current. Steep topography: horizontal scale $\leq$ width of the current.
- Straight fronts with velocity in geostrophic balance: exact solutions. Linear stability: collocation method. Unstable modes: resonances between eigenmodes.
- Unstable modes $\rightarrow$ initialization of numerical simulations with new-generation well-balanced high resolution finite-volume scheme (Bouchut & Zeitlin 2010).

Coupled density fronts with nontrivial bathymetry

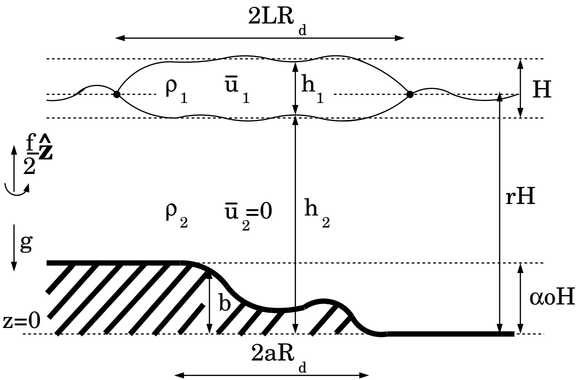

R_d: deformation radius, L and a: nondimensional widths of the balanced current and of the escarpment. r: depth ratio, α_0: non-dimensional amplitude of the bathymetry.

Equations of the model

$$
\begin{aligned}
(\partial_t + u_i\partial_x + v_i\partial_y)u_i - fv_i + \partial_x\Pi_i &= 0 \quad , \\
(\partial_t + u_i\partial_x + v_i\partial_y)v_i + fu_i + \partial_y\Pi_i &= 0 \quad , \\
\partial_t h_i + \partial_x((h_i - b\,\delta_{i2})u_i) + \partial_y((h_i - b\,\delta_{i2}v_i) &= 0 \quad .
\end{aligned} \tag{1}
$$

u_i, v_i $(i = 1, 2)$ - x- and y- components of the velocity in the layers (layer 1 on top of the layer 2); h_1, $h_2 - b$ - thicknesses of the layers, δ_{ij} -Kronecker delta; $\rho = \frac{\rho_1}{\rho_2} \leq 1$ - density ratio, $f = const$ - Coriolis parameter, g - gravity. Geopotentials of the layers $(1, 2)$:

$$
\Pi_1 = g(h_1 + h_2) \quad , \quad \Pi_2 = g(\rho h_1 + h_2). \tag{2}
$$

Intrinsic scales:

- Length: radius of deformation $R_d = \sqrt{gH(1-\rho)}/f$,
- Time: $1/f$.
- dimensionless wavenumber $\epsilon = 2\pi R_d/\lambda$

Scalings:

- cross-stream coordinate $y \sim R_d$,
- downstream coordinate $x \sim \lambda/2\pi = R_d/\epsilon$
- time $t \sim 1/\epsilon f$.
- width of the current: $2R_d L$, $L = \mathcal{O}(1)$.
- bathymetry variations: $R_d a$
- cross-stream velocities $\sim \epsilon\sqrt{gH(1-\rho)}$, and downstream velocities $\sim \sqrt{gH(1-\rho)} \Rightarrow Ro = \frac{1}{2L}$.

Non-dimensional equations of the model

$$
\begin{aligned}
(\partial_t + u_i\partial_x + v_i\partial_y)u_i - v_i + \partial_x\Pi_i &= 0 \quad , \\
\epsilon^2(\partial_t + u_i\partial_x + v_i\partial_y)v_i + u_i + \partial_y\Pi_i &= 0 \quad , \\
\partial_t h_i + \partial_x((h_i - \tfrac{\alpha_0}{r} b\,\delta_{i2})u_i) + \partial_y((h_i - \tfrac{\alpha_0}{r} b\,\delta_{i2})v_i) &= 0 \quad ,
\end{aligned} \tag{3}
$$

$$
\Pi_1 = \frac{h_1 + rh_2}{1-\rho} \quad , \quad \Pi_2 = \frac{\rho h_1 + rh_2}{1-\rho} \quad .
$$

Backround flow

Background flow $(\bar{u}_i, \bar{v}_i, \bar{h}_i)$ is a geostrophically balanced, parallel to the $x-$axis density current terminating at $\pm L$, with no mean flow in the lower layer:

$$\bar{u}_1 = \bar{u} = -\partial_y \bar{h} \quad , \quad \bar{\Pi}_1 = \bar{h} \quad , \quad \bar{\Pi}_2 = 0 \quad , \quad \bar{u}_2 = \bar{v}_2 = \bar{v}_1 = 0 \quad . \tag{4}$$

$\bar{h}_1 = \bar{h}$ is the background thickness of the upper layer, $\bar{h}(\pm L) = 0$, otherwise $\bar{h}(y)$ is arbitrary There is no variation of bathymetry beyond the outcroppings $a < L$:

$$\begin{aligned} b = 1 \quad &, \quad y < -a \quad , \\ b = 0 \quad &, \quad y > a \quad . \end{aligned} \tag{5}$$

Constant-PV currents

If potential vorticity is constant Q in the upper layer, $\partial_{yy}\bar{h} - Q\bar{h} + 1 = 0$, and

$$
\begin{aligned}
Q < 1 : \quad & \bar{h} = \frac{1}{Q}\left(1 - \frac{\cosh(y\sqrt{Q})}{\cosh(L\sqrt{Q})}\right) \quad , \quad L = \frac{1}{\sqrt{Q}} \ln\left(\frac{1+\sqrt{Q(2-}}{1-Q}\right. \\
Q < 0 : \quad & \bar{h} = \frac{1}{Q}\left(1 - \frac{\cos(y\sqrt{|Q|})}{\cos(L\sqrt{|Q|})}\right) \quad , \quad L = \frac{1}{\sqrt{|Q|}} \cos^{-1}\left(\frac{1}{1+|Q|}\right) \\
Q = 0 : \quad & \bar{h} = 1 - (y/L)^2 \quad , \quad L = \sqrt{2}
\end{aligned}
\tag{6}
$$

For $Q = 0.5$ - a configuration to be used below for illustrations, $L \simeq 1.86$ and $Ro \simeq 0.27$.

Cross-section of the background flow

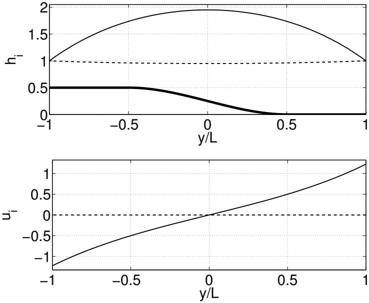

Background flow for constant PV $Q = 0.5$ in the upper layer. Density ratio $\rho = 0.5$. Depth ratio $r = 10$. Topography: $\alpha_0 = 5$ and $a = 0.5L$. *Upper panel:* interface (dashed), free surface (solid) and topography (thick). *Lower panel:* downstream velocities of the layers 2 (dashed) and 1 (solid).

Boundary conditions

Linear stability: small perturbation (u_i', v_i', h_i').

Boundary conditions:

$$\bar{h} + h_1' = 0 \quad \text{and} \quad \frac{\mathrm{d}L_\pm}{\mathrm{d}t} = v_1' \quad \text{at} \quad y = \pm L + \lambda_\pm \quad , \tag{7}$$

$\pm L$ - locations of the free streamlines of the balanced flow, $\lambda_\pm(x, t)$ - perturbations of the free streamlines. Another boundary condition: for the lower layer, the continuity of the solution at $\pm L$.

Beyond the outcropping: exponential decay of the pressure perturbation on both sides of the double front $\Rightarrow$ boundary conditions at the outcroppings $\Rightarrow$ entire linear eigenproblem solely at the interval $y \in [-L, L]$.

Comment on boundary conditions

Spectrum of the linearized problem in the cross-flow direction: discrete + continuous. First: free inertia-gravity waves. Second: trapped waves exponentially decaying out of the density fronts. By imposing the decay boundary condition we filter out free inertia-gravity waves and concentrate uniquely on the trapped modes - consistent with our interest in long-wave instabilities. Only the instabilities resulting from the resonances between the trapped modes will be captured, radiative instabilities due to the resonances with free inertia-gravity waves are excluded. *A priori* justification: condition of efficient emission of inertia-gravity waves by a PV anomaly is $Ro \geq 1$, while we work with $Ro < 1$. *A posteriori* justification: no radiative instabilities observed in DNS.

Numerical linear stability analysis

- Method: pseudospectral collocation (Trefethen 2000) $\rightarrow$ matrix eigenproblem for the phase speed c of the perturbation, MATLAB routine "eig",
- Boundary conditions: continuity of all variables at $y = \pm L$, continuity of the lower-layer pressure at $y = \pm L$ and exponential decay out of the front,
- Discretization: Chebyshev collocation points $\{y_i = L\cos(j\pi/N),\ j = 0, 1, .., N\}$. Numerical convergence typically for N=50, systematic checks with double resolution. Chebyshev differentiation matrix for discrete differentiation,
- Topography: escarpment with a linear slope,
- Treatment of spurious soloutions (singular modes): filtering based on slope limiters + increase of resolution.

Wave species of the flow

Flow with constant Q in the upper layer and bottom escarpment:

- Poincaré (inertia-gravity) modes in both layers,
- Rossby modes in the lower layer (no PV gradients in the upper layer),
- Frontal modes, trapped in the vicinity of the free streamlines in the upper layer,
- Topographic waves in the lower layer, trapped by the varying bathymetry.

Instabilities: resonances between the eigenmodes of the linearized problem. Resonances $\leftrightarrow$ crossings of dispersion curves (Cairns 1979).

Expectations

Expect following resonances and related instabilities :

1. the barotropic resonances of the upper-layer modes between :
   - two frontal waves (FF);
   - a Poincaré and a frontal wave (P1F);
   - two Poincaré waves (P1P1).
2. the baroclinic resonances of the modes of different layers between:
   - a frontal upper wave and a lower Rossby wave (RF);
   - a frontal upper wave and a lower topographic wave (TF);
   - an upper Poincaré wave and a lower Rossby wave (P1R);
   - an upper Poincaré wave and a lower topographic wave (P1T);
   - a frontal upper wave and a lower Poincaré wave (P2F);
   - upper and lower Poincaré waves (P1P2).

Stability diagram: very deep lower layer with $Q = 0.5$

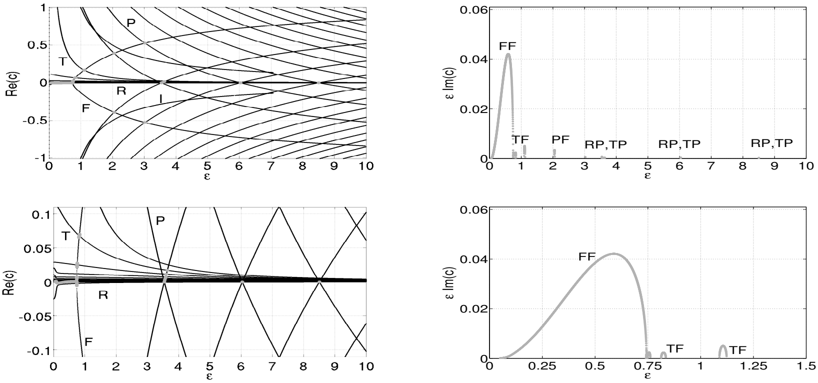

Density ratio $\rho = 0.5$. Depth ratio $r = 100$. Topography: $a = 0.5L$, $\alpha_0 = 50$. *Gray:* unstable. *Black:* stable. *Waves:* I - inertial; F - frontal; R - Rossby, T - topographic. *Bottom:* zoom.

Most unstable mode: FF resonance

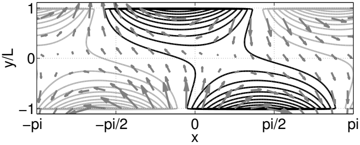

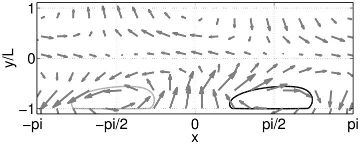

2D structure of the most unstable mode ($\epsilon = 0.59$): resonance between two frontal waves in the upper layer. *Left:* Isobars (contour interval 0.05) and velocity field of the perturbation in the upper layer. *Right:* Isobars (contour interval 0.001, starting from ± 0.001) and velocity field of the perturbation in the lower layer. Positive (negative) pressure anomalies: black (gray) lines. $\|\mathbf{v_2}\|_{max} \simeq 0.003\|\mathbf{v_1}\|_{max}$.

Stability diagram: moderately deep lower layer

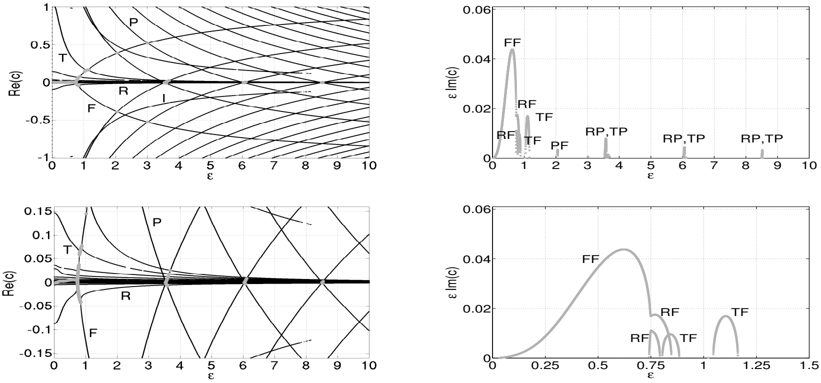

Same background flow with the depth ratio $r = 10$ and the topography parameter $\alpha_0 = 5$. *Bottom:* zoom in the stability diagram.

Second unstable mode: RF resonance

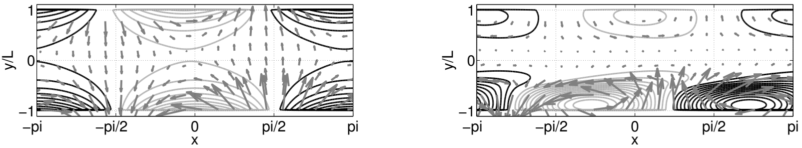

2D structure of the unstable mode with $\epsilon = 0.77$. Resonance between a frontal wave (*upper layer*) and a Rossby wave (*lower layer*). Perturbation with $Re(c) < 0$. $\|\mathbf{v_2}\|_{max} \simeq 0.035\|\mathbf{v_1}\|_{max}$.

Next unstable mode: TF resonance

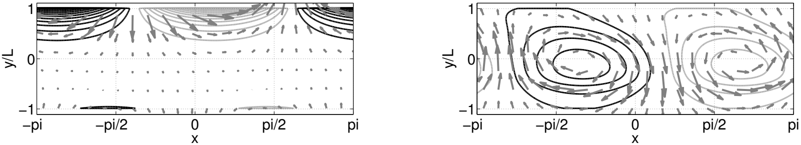

2D structure of the unstable mode with $\epsilon = 1.105$. Resonance between a frontal wave (*upper layer*) and the first topographic mode (*lower layer*). Isobars of the perturbation in the lower layer (contour interval 0.005, starting from ± 0.005). $\|\mathbf{v_2}\|_{max} \simeq 0.05 \|\mathbf{v_1}\|_{max}$.

Unstable mode corresponding to TF resonance with second topographic mode

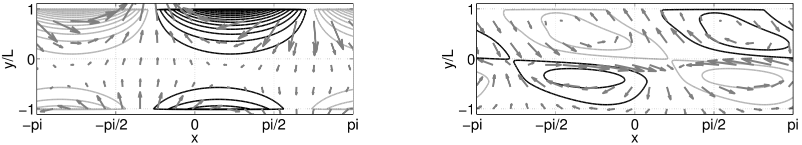

2D structure of the unstable mode with $\epsilon = 0.842$. Resonance between a frontal wave (*upper layer*) and the second topographic mode (*lower layer*). $\|\mathbf{v_2}\|_{max} \simeq 0.035\|\mathbf{v_1}\|_{max}$.

Unstable mode corresponding to P1R resonance

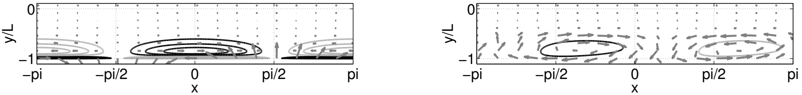

2D structure of the unstable mode with $\epsilon = 3.577$. Resonance between a Poincaré mode in the upper layer and a Rossby wave in the lower layer. Perturbation $Re(c) < 0$. Isobars of the perturbation in the lower layer (contour interval 0.0005, starting from ± 0.0005). $\|\mathbf{v_2}\|_{max} \simeq 0.0055 \|\mathbf{v_1}\|_{max}$.

Stability diagram: shallow lower layer

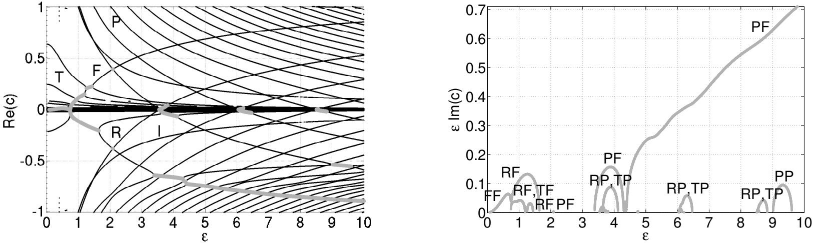

Stability diagram for the same background flow with the depth ratio $r = 2$ and the topography parameter $\alpha_0 = 1.4$.

Unstable mode corresponding to P2F resonance

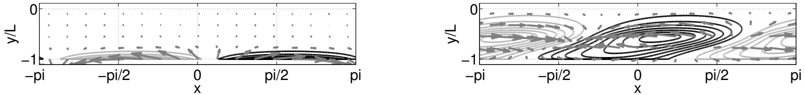

2D structure of the unstable mode with $\epsilon = 3.885$. Resonance between a Poincaré mode in the lower layer and a frontal wave in the upper layer. Perturbation with $Re(c) < 0$. Isobars of the perturbation in the lower layer (contour interval 0.01, starting from ± 0.01). $\|\mathbf{v_2}\|_{max} \simeq 0.27 \|\mathbf{v_1}\|_{max}$.

Example of competing instabilities

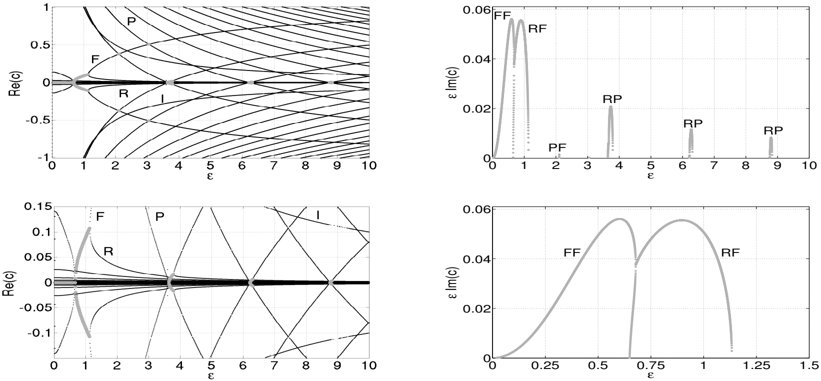

Stability diagram for the flat-bottom background flow with $Q = 0.6$, $\rho = 0.5$, and depth ratio $r = 2$. *Bottom:* zoom in the stability diagram.

Motivations/questions

- how the active lower layer influences the nonlinear evolution of the coupled density fronts established in the framework of equivalent 1-layer model (Scherer & Zeitlin 2008)?
- what are the differences in saturation of (*FF*) instability and of its rival, the (*RF*) instability?
- how the presence of the second density front/absence of the boundary (coast) influences the saturation of the (*RF*) instability observed in the case of the coastal current with similar settings (Gula, Zeitlin & Bouchut2010)?
- how the presence of escarpment beneath the fronts changes the scenarii of saturation?

Numerical settings

Numerical scheme:

Finite-volume, well balanced, shock-capturing for 2-layer RSW with free upper surface (Bouchut & Zeitlin 2010).

Initialization/resolution:

- Initialization: basic flow + perturbation of the amplitude $\approx 1\%$ of the max thickness of the unperturbed upper layer. Perturbation: an unstable mode.
- Boundary conditions: sponges cross-stream, periodicity downstream.
- Resolution: typically 0.067 R_d, control simulations with double resolution

Caveats of 2-layer model:

- Strong vertical shears $\Rightarrow$ loss of hyperbolicity (physically: KH instabilities). Numerical scheme copes well with them: strong gradients trigger enhanced numerical dissipation and the scheme cures itself, the non-hyperbolic zones remaining localized and eventually disappearing.
- Rankine-Hugoniot conditions for the model are not complete, extra *ad hoc* hypotheses are needed to determine weak solutions (shocks). Our scheme: layerwise momentumn conservation

Benchmark: comparison with the results of the linear stability analysis

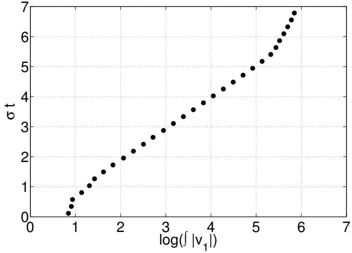

Comparison of the growth rate of the *FF* instability at the initial stages of the direct numerical simulation initialized with the most unstable mode with the predictions of the linear stability analysis: logarithm of the norm of the cross-stream velocity in the upper layer vs time normalized by the linear growth rate.

Nonlinear evolution of the *FF* instability

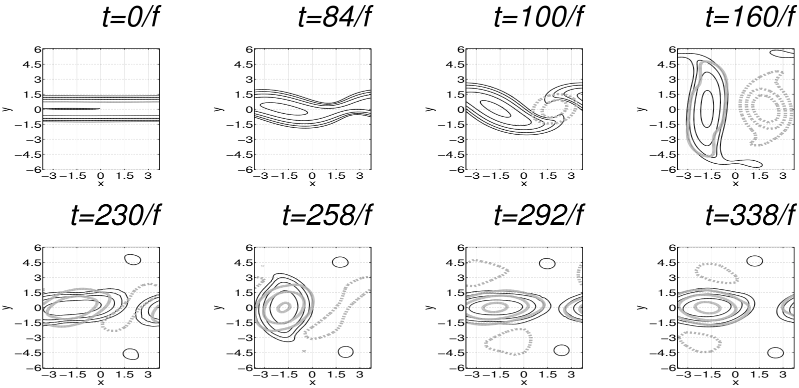

Thickness h_1 of the upper layer (*black*). Contour interval 0.2, starting at 0.2. Pressure Π_2 *(gray)* of the lower layer. Contour interval 0.05, starting at $rH \pm 0.05$ (*+/- anomaly: solid/dashed*).

Energy balance of saturating *FF* instability

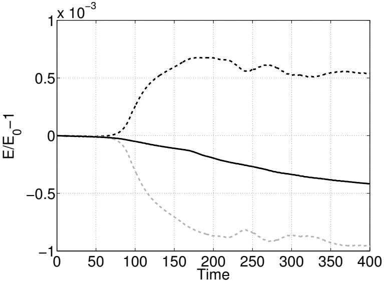

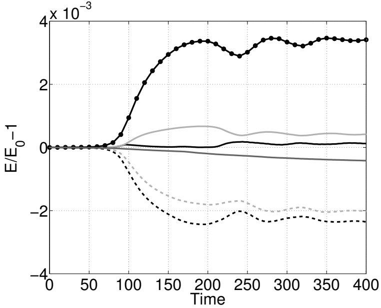

Left: Normalized deviation of the total *(solid)*, kinetic *(black dashed)* and potential *(gray dashed)* energy from initial values. *Right:* Normalized deviations of the kinetic $\rho_i h_i/2\mathbf{v_i}^2$ *(solid)* and potential $\rho_i g h_i^2/2$ *(dashed)* of layers 1 *(black)* and 2 *(gray)*. Exchange $\rho_1 g h_1 h_2$ *(solid dotted)* and total *(dark gray)* energies.

Nonlinear evolution of the *RF* instability

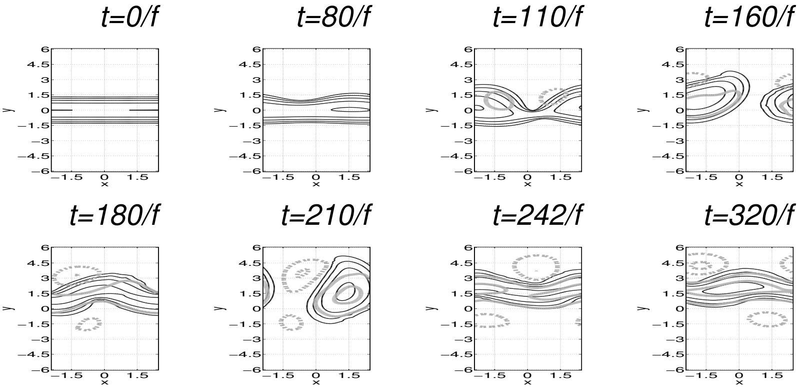

Thickness h_1 of the upper layer (*black*). Contour interval 0.2, starting at ± 0.2. Pressure Π_2 *(gray)* of the lower layer. Contour interval 0.05, starting at $rH \pm 0.05$ (*+/- anomaly: solid/dashed*).

Energy balance of saturating *RF* instability

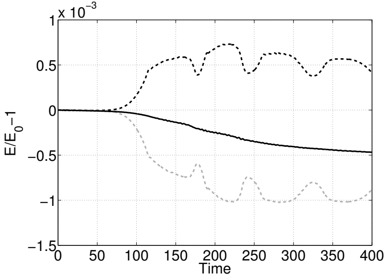

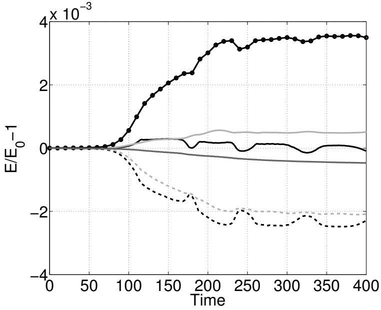

Left: Normalized deviation of the total energies from their initial values.
Right: Evolution of different energy components.

Saturation of *FF* instability over escarpment

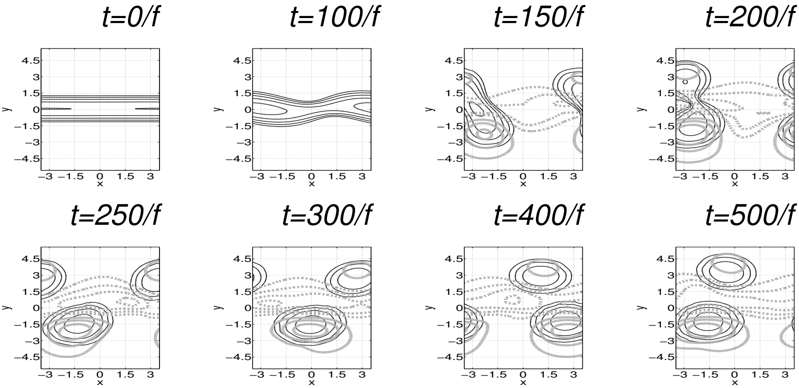

Thickness h_1 of the upper layer (*black*). Contour interval 0.2, starting at ± 0.2. Pressure Π_2 *(gray)* of the lower layer. Contour interval 0.015, starting at $rH \pm 0.015$ (*+/-: solid/dashed*).

Saturation of *RF* instability with topography

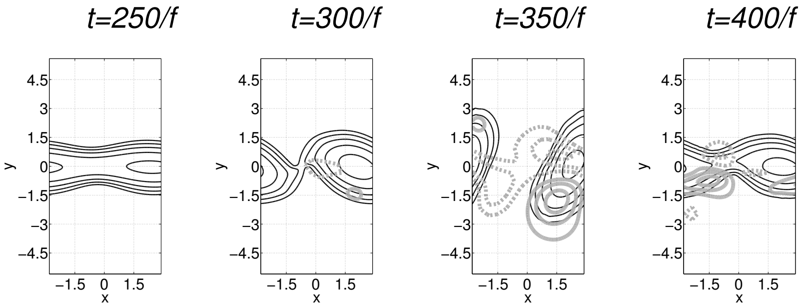

Nonlinear evolution of the *RF* instability over escarpment. Thickness h_1 of the upper layer (*black*). Contour interval 0.2, starting from 0.2. Pressure Π_2 *(gray)* of the lower layer. Contour interval 0.01, starting at $rH \pm 0.01$ (positive/negative pressure anomaly: *solid/dashed*).

Nonlinear development of the *TF* instability

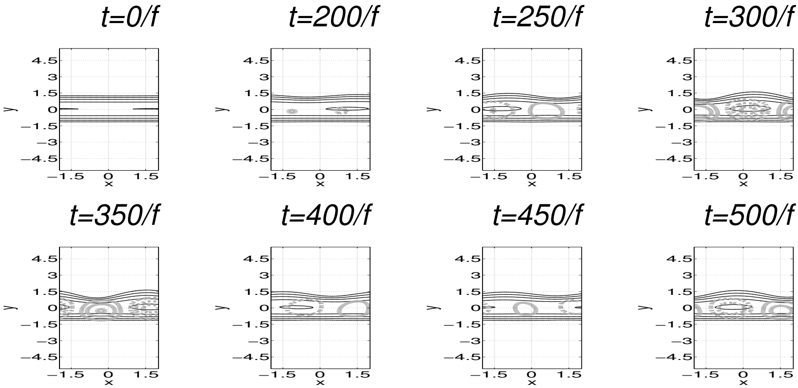

Thickness h_1 of the upper layer (*black*). Contour interval 0.2, starting at 0.2. Pressure Π_2 *(gray)* of the lower layer. Contour interval 0.005, starting at $rH = \pm 0.005$ (*+/- : solid/dashed*).

Energy balance of *TF* instability

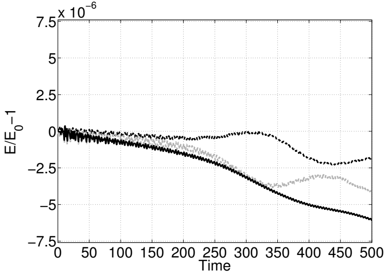

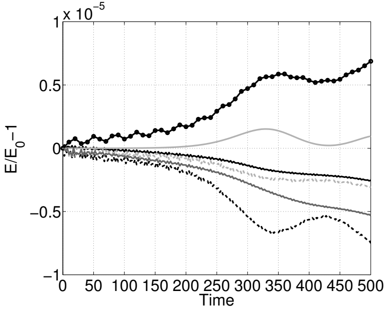

Energy balance of the developing *TF* instability: extremely small dissipation.

Linear stability analysis:

- Leading long-wave barotropic *FF* instability dominant for deep lower layers, may be overcome by the baroclinic *RF* instability when the depth of the lower layer decreases, including asymmetric decrease in depth due to topography. Topography renders the *FF* instability propagative.
- Specific long-wave topographic *TF* instability arises. In the configuration with centered escarpment it is never dominant.
- For shallow (partially shallow due to topography) lower layers short-wave Kelvin-Helmholtz type instabilities become dominant.

Nonlinear saturation of long-wave instabilities:

- *FF* instability over the flat bottom saturates by reorganizing the flow in a system of co-rotating ellipsoidal quasi-barotropic vortices, the rodons.
- *FF* instability over escarpment saturates by reorganizing the flow into two rows of quasi-circular quasi-barotropic vortices on both sides of the escarpment.
- *RF* instability saturates by forming transient upper-layer monopolar and lower-layer dipolar vortices which, after a stage of a sideward motion reorganize themselves in a secondary mean current, shifted with respect to the initial one and experiencing subsequent secondary instabilities.
- *TF* instability saturates forming a steady finite-amplitude nonlinear hybrid fronto-topographic wave